J. Phys. D: Appl. Phys. 27 (1994) 1252–1266. Printed in the UK

Theoretical modelling of the development of the positive spark in long gaps

A Bondiou† and I Gallimberti‡

† Office National d'Etudes et Recherches Aerospatiales, Chatillon s/ Bagneux, France
‡ Department of Electrical Engineering, University of Padua, Italy

Received 19 October 1992, in final form 6 December 1993

Abstract. The main purpose of this paper is to present a physical model of the positive discharge in long air gaps. A large number of previous experimental and theoretical studies led to the identification of the different successive phases of the spark development: formation and propagation of first corona streamers, inception of the conductive stem at the electrode tip, formation and development of second corona (or 'leader corona') from the stem, and, eventually, the propagation of the leader and leader corona system until the final jump preceding the arc onset. Details of the specific modelling of each phase is presented, using the classical equations for conservation of mass, momentum and energy for each particle species. These basic equations are simplified according to the dominant electrostatic, hydrodynamic or thermodynamic processes involved in each step of the spark development. The resulting models for simulation of the corona and leader phases are coupled with an analytical calculation of the electric field due to the electrodes, the leader channel and the space charge injected into the gap. The different phase simulation models are expressed with a homogeneous simplification level and then linked sequentially into a complete model, which performs the step-by-step simulation of all the successive discharges phases until the final jump. The model described here is self-consistent since the only input data are the electrode geometry and the applied potential wave-shape. A good agreement between computed and experimental results has been obtained in various test configurations; the model has been also used to simulate the discharge behaviour with perturbations of the applied potential wave and permits the analysis of the conditions for stable propagation of the positive leader. It is shown that some parameters of practical interest, as the 50% breakdown voltage or the time to breakdown can be derived from the proposed model.

1. Introduction

Discharges over long air gaps can be characterized by their ability to propagate in low electric fields by reproducing self-sustained conditions across the gap during their development. Experimental studies of the dielectric properties of long air gaps showed that the breakdown characteristics are highly nonlinear, depending on the different electrode configurations and the various voltage waveforms applied to the gap. For this reason, several theoretical studies have been carried out in order to obtain self-consistent predictive modelling of the various phases of the discharge development.

In the last 20 years, the basic physical processes of the discharge have been investigated with the help of several experimental programmes, a great deal of this work being realized by the Les Renardiéres Group (Les Renardiéres Group 1972, 1974, 1977, 1981). These experimental studies allowed one to define the different subsequent phases of the breakdown process and pointed out the evolution of plasma properties (such as temperature and charged particle densities), which characterize the transition between them.

A large set of theoretical studies dealt with specific modelling of these various phases (Meek and Craggs 1978, Gallimberti 1979, Les Renardières Group 1986). These models are based on general descriptions of the basic physical processes and state some simplifying assumptions, according to the dominant phenomena, which lead to various degrees of complexity in the mathematical formulation.

The first aim of the present work is to modify these different models in order to put them on a homogeneous simplification level and, when possible, to use analytical expressions instead of numerical solutions, in order to avoid too long a computation time. In a second stage,

0022-3727/94/061252+15$19.50

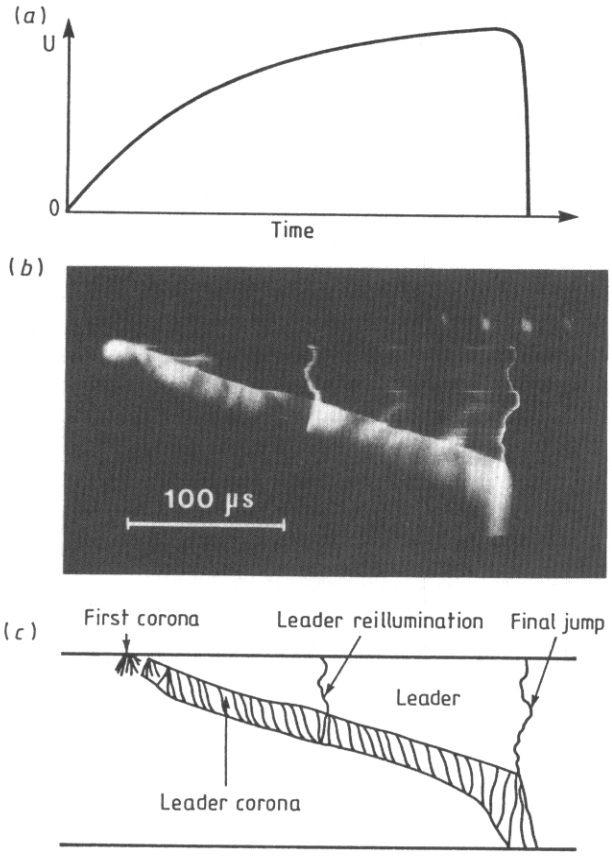

Figure 1. (*a*) Voltage waveform applied to the gap. (*b*) Streak photograph of a long spark developing in a positive point-to-plane gap. (*c*) Schematic representation of the discharge of (*b*).

these partial models are linked into a single and general model of spark development: the output of each basic section is then used as the input for the following one in order to simulate in sequence the different phases of the discharge. The final purpose is to provide a single analytical model, which needs the gap geometry and voltage waveform as input data. This model, which includes specific analysis of instabilities and arrest conditions, describes the discharge development until the onset of the final jump.

The reference configuration used in these calculations is a non-uniform long gap (point–plane) subjected to positive impulse voltages.

2. Description of the discharge development

The main chronological sequence of events that occur when a positive voltage waveform (figure 1(*a*)) is applied to a non-uniform gap can be derived from the streak photograph of figure 1(*b*), which also gives a general schematic representation of the spark structure (figure 1(*c*)).

Above a minimum voltage threshold, the discharge process is initiated with the formation of the 'first corona', which takes the form of filamentary branched channels ('streamers'), developing from a common root ('stem'). The associated current pulse consists of a steep increase in a few tens of nanoseconds, followed by a longer exponential decay. The radius of the streamer filament was estimated in the range 10–30 μm (Marode 1972). Strioscopic and spectroscopic analyses indicate that streamers are 'cold' discharges as the neutral temperature is around the ambient value (Hartmann 1977). The streamer structure includes an active region (streamer head), in which ionization processes take place, and a passive region (streamer channel), in which the electrons drift and become attached to electronegative molecules (Marode 1975, Marode *et al* 1978). The advancement process is related to the concentration of positive ions at the filament tip: this causes a space charge field high enough to sustain the development of electronic avalanches in the active region. This electrostatic mechanism enables the propagation of the active region in external geometric fields much lower than the critical value (at which ionization and attachment rates become equal), without any thermodynamical mechanism being involved.

Depending on the value of the curvature radius of the HV electrode, a dark period of various durations takes place after the first corona. The subsequent phase of the discharge is the inception and development of the 'second corona'; this phase also includes the inception of the 'leader channel' from the stem, which appears as a brighter filamentary zone advancing at the root of the streamer bush.

The charge injected in the gap by the first corona produces a field distortion, which reduces the applied field and delays the inception of the second corona; at the same time, this injected charge induces the physical processes for the evolution of the stem into the leader channel. The dominant mechanism for this transition is Joule heating due to the streamer current flowing along the stem channel: above a critical temperature around 1500 K thermal detachment of negative ions enhances the conductivity and lowers the internal field, leading to formation of the first leader section and to a field increase at the stem tip, which causes inception and development of the second corona.

The leader channel then starts to propagate with the 'leader corona' developing in front of its head. The leader head appears as a propagating thermal transition wave, which converts the cold diffuse glow of the leader corona into a hot filamentary discharge of relative high conductivity. The ionization activity at the front of the leader corona streamers supplies the current and energy input necessary to sustain the thermal transition at the leader head; conversely, the advancement of a conductive channel into the gap sustains the potential and the field in the streamer front making possible its continuous advancement. The leader appears as a thin filamentary channel, which expands in time. Strioscopic experiments (Ross 1977) have given the size of the channel radius, which is around 1 mm. The propagation of the streamer–leader is mainly continuous except in high ambient air humidity conditions where strong discontinuities or 're-strikes' take place (see figure 1(*b*)). In the stable propagation conditions, the

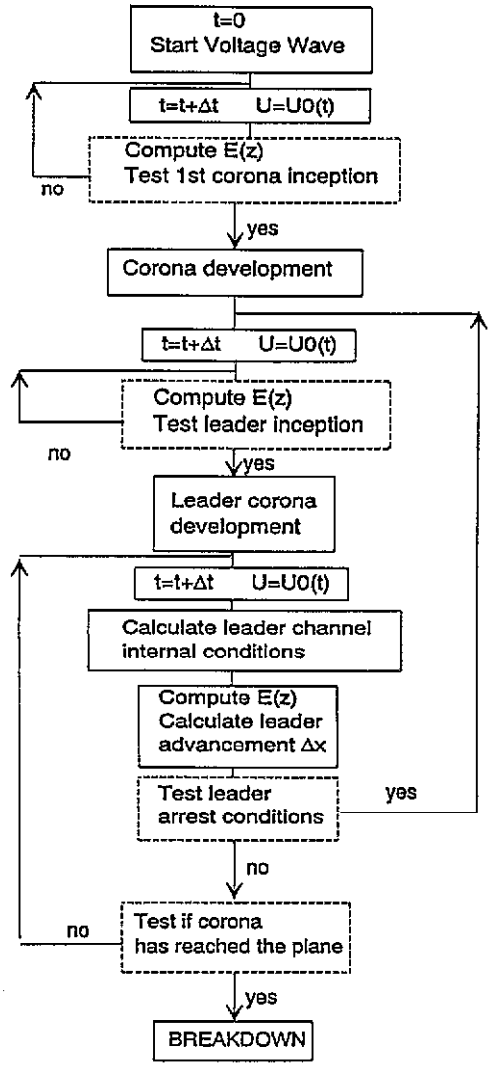

Figure 2. General flow-chart of the model.

leader is associated with a low current, below 1 A and the electric field in the channel remains within the range 1–5 kV cm^{-1}. Spectroscopic analysis of the emitted light (Les Renardières Group 1977) has shown that the neutral temperature in the channel is in the range 2000–6000 K: this indicates a non-LTE state of the plasma and excludes thermal ionization processes.

Propagation continues until the corona streamers reach the earthed plane. The subsequent final jump and arc phases will follow inevitably. However, these phases will not be described in this model, as its main interest is the determination of breakdown conditions for which purpose simulation of the discharge development until it reaches the plane is sufficient.

3. General principles of modelling

The model of the discharge processes in long gaps (see the general flow-chart of figure 2) is a self-consistent time-dependent model: the input data are only the geometry of the electrodes and the voltage wave-shape.

The discharge time-base is divided in steps Δt, starting from $t = 0$; at each time step, the applied voltage $U_0(t)$ is calculated, together with the electric field distribution in the gap; the first corona inception conditions (minimum threshold voltage and statistical time lag) are tested until they are satisfied. At this instant, the first corona development in the actual electric field is simulated, and its size, current and charge are calculated.

After the first corona formation, the field calculation at each time step includes the positive space charge left in the gap by the corona itself. The leader inception conditions (temperature inside the stem and electric field at its tip) are tested until they are both satisfied. At this time, the second corona development from the stem tip is simulated and its size, current and charge are calculated.

After formation of the second corona, propagation of the continuous streamer–leader system is started; at each time step, the internal conditions of the leader channel (temperature, radius, electron density and electric field) are calculated and the voltage drop along the leader channel is evaluated. According to the actual values of leader length, voltage drop along the channel and total corona charge, the electric field distribution is recalculated; on this basis, the propagation characteristics of the advancing streamer front are calculated, together with the leader current and advancement velocity.

At each time step, the critical conditions for leader or streamer arrest are tested: if not satisfied, the programme continues the propagation loop, until the start of the final jump, when the streamer front reaches the plane. If the streamer–leader system stops, new inception conditions are required, until the system starts again or stops definitively after the voltage crest.

In general, the different phases may be described as the formation and evolution of inhomogeneous, non-equilibrium plasma regions, which contain charged and neutral particles. For each species, the conservation equations for mass, momentum and energy must be solved together with Poisson's equation and Ohm's law (current density equation).

The analysis of the characteristic time constants of the physical mechanisms involved leads to great simplifications of these equations that vary among the different cases (Gallimberti 1979).

4. Calculation of the electric field along the propagation axis

Calculation of the electric field during discharge evolution has to take into account the geometric and electrostatic structure of different parts of the discharge (corona and leader) and the induced charges on the electrodes.

The proposed method assumes that both electrodes and discharge have a rotational symmetric configuration and that the corona and streamer–leader system can be represented by space charge distributions whose geometry is defined by the applied potential surfaces. Figure 3 gives a simplified sketch of the discharge geometry for a rod–plane gap of length D and an

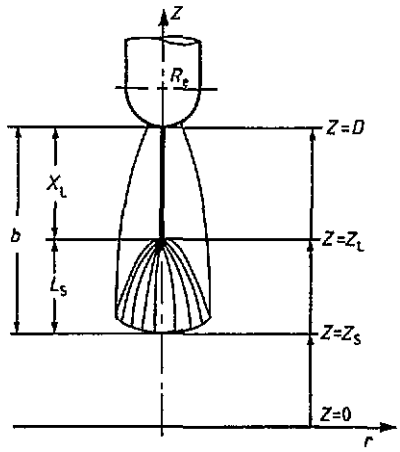

Figure 3. *General scheme of the discharge simplified* geometry, with indication of the streamer front coordinate Z_s, leader tip coordinate Z_L, leader and corona lengths X_L and X_s, and space-charge region length b.

electrode tip curvature radius R_e and for given positions Z_s and Z_l of the streamer–leader system in the gap. In the reference rod–plane configuration, these distributions are easily represented in an ellipsoidal–hyperboloidal coordinate system, originating at the ground plane, with the focal point on the rod centre. This allows an analytical solution of Poisson's equation and is consistent with the main geometrical characteristics of the discharge. The field distribution is the sum of the following contributions.

(i) Field due to electrodes and leader channel, in the absence of space charge. The HV electrode has a potential U_0 and, due to its longitudinal field E_{ch}, the leader tip has a potential $U_{lt} = U_0 - X_l E_{ch}$ lower than U_0.

(ii) Field produced by the coronal space charge.

(iii) Field produced by the surface charges induced by the corona charge on the ground plane, the HV electrode and the leader channel.

Detailed calculation of each field component has been described by Gallimberti *et al* (1982, 1983).

5. Inception and development of the corona phase

In the original streamer theory proposed by Raether (1939) and Loeb and Meek (1941), the tip of a streamer filament is assumed to be the front of a space charge wave, where positive ions and excited molecules, produced by previous ionization and excitation phenomena, are highly concentrated. The decay of the excited states induces, by photo-ionization, a distribution of secondary electrons around the wavefront. If the total electric field (geometric plus space charge components) is high enough, these free electrons will develop electron avalanches when drifting in the field direction.

Theoretical (Dawson and Winn 1965) and experimental works (Phelps 1971) have studied the minimum external field required to sustain an energetically stable propagation: the result is of the order of 4–5 kV cm^{-1} at 1 bar, depending essentially on humidity conditions. Gallimberti (1972a) has developed a model of streamer propagation, which solves in a simplified way the set of continuity equations for electrons, positive and negative ions, together with Poisson's equation. The streamer advancement capability results from the balance between energy losses in electron–neutral species collisions, energy gain due to the applied field and variations of the space charge potential energy.

In order to reduce the computation time, it is possible to develop a simplified model, by representing the series of avalanches through a single 'equivalent avalanche', under the condition that this equivalent avalanche produces the same space charge as the series of avalanches: the energy balance equation can be therefore used as an equivalence condition (Gallimberti 1972a), and the streamer propagation can then be described step-by-step by the successive equivalent avalanches.

5.1. The criterion for streamer inception

As criterion for inception and propagation, it assumed that the ionic charge in the streamer head N_s must be higher than a minimum 'stability charge' N_{stab}, defined as the minimum charge that produces a space charge field high enough to reproduce the streamer tip. The use of Gallimberti's model enables the computation of N_{stab} as a function of the external field at the streamer tip E_{gs} (Badaloni and Gallimberti 1972). The inception of a stable streamer implies that the size of the initial equivalent avalanche is greater than or equal to N_{stab}. *The condition can be expressed by the following relation:*

$$\exp\left[\int_{\Delta x} (\alpha - \eta)\,dx\right] > N_{stab} \qquad (1)$$

where α is the ionization coefficient; η is the attachment coefficient and Δx is the size of the active region where $\alpha - \eta > 0$.

The ionization and attachment coefficients are computed as functions of the local field. Equation (1) can be used to study the corona inception provided the electric field distribution is known.

5.2. A simplified model of streamer development

A simplified version of the streamer model has been developed (Badaloni *et al* 1992) in order to predict corona characteristics using analytical formulae and to describe streamer features as functions of the space coordinate x (curvilinear coordinate along the geometric field line that guides streamer propagation). If the streamer head radius R is assumed to be constant during propagation, the energy balance at the streamer front leads to a continuous relation giving the number of

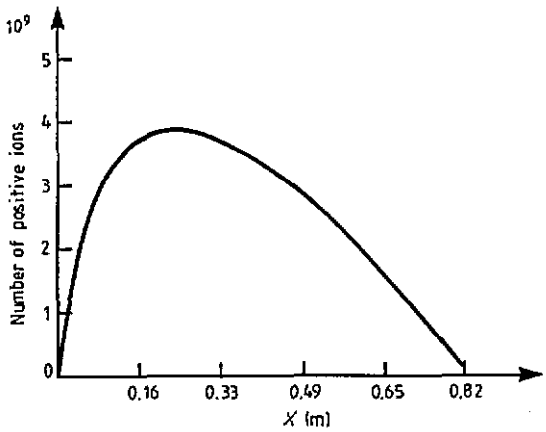

Figure 4. Simplified model of the development of a streamer in a rod–plane gap (first corona case). Computed potential number of positive ions in the active head $N(x)$. Gap length $D = 10$ m, rod curvature radius $R_e = 0.1$ m and electrode potential at inception time $U_i = 800$ kV.

positive ions $N_s(x)$ in the streamer head as a function of the x coordinate:

$$N_s(x) = \frac{2eR+\mu}{4a}\left(V_0 + \frac{4a}{2eR+\mu}N_0 - \frac{\beta}{2eR+\mu}x - V(x)\right) \tag{2}$$

with $V(x)$ is the potential distribution along the guiding field line (V_0 is the potential at $x = 0$), N_0 is the value of $N_s(x)$ at $x = 0$, β and μ are coefficients for energy loss and gain and $a = 0.4e^2/(4\pi\epsilon_0)$.

It can be seen from equation (2) that the stability condition $\partial N/\partial x = 0$ provides an analytical expression for the stability field $E_{gs} = \partial V/\partial x$ as a function of R, β and μ. The result is of the order of 4–5 kV m^{-1} as is experimentally observed.

Streamer propagation stops at a maximum distance x_s when the number of ions in the streamer head $N_s(x)$ becomes lower than the stability charge N_{stab}. The length of the corona can then be obtained using the simple relation

$$N_s(x_s) = N_{stab}(E_g(x_s)).$$

The evolution of $N_s(x)$ for development of a first corona in a rod–plane gap is given in figure 4.

5.2.1. Calculation of the corona charge. The total net space charge Q generated by the streamer formation corresponds to the total number of electrons that have left the gap by reaching the HV electrode (the conduction current component). It can be therefore calculated (Badaloni *et al* 1992) as

$$Q = e\int_0^{x_s} \frac{N_s(x)}{2R}\exp(-\eta x)\,dx \tag{3}$$

where η is the attachment coefficient.

The charge Q is associated with the development of a single streamer filament; the total corona charge Q_c is then obtained by multiplying the individual charge Q by a branching factor f_b and by the number of filaments N_f. The branching factor f_b has been studied theoretically (Badaloni and Gallimberti 1973) using a Monte Carlo method in order to estimate the number of streamer branches that develop during the propagation. It has been shown that the actual charge is increased by the branching process by a factor of approximately five, over a very large set of laboratory configurations. The number N_f of filaments represents the number of streamer starting points on the electrode surface, which increases with electrode radius and with overvoltage ratio. Guidelines for its value can be deduced from current measurements in different electrode geometries (Les Renardières Group 1972, 1974, 1977). First and second corona have been treated identically, with the same values for N_f and f_b.

5.2.2. Calculation of the associated current. The corona current I, which is injected into the gap by the external circuit during corona development, can be calculated from the Shockley–Ramo theorem:

$$V_0 I = \iiint_v e(n_+v_+ + n_-v_-)E_g\,dv \tag{4}$$

with E_g the geometric electric field at a given point of the discharge volume V and n_+, v_+, n_- and v_- the corresponding density and velocity of positive ions and electrons.

The individual streamer current has two components (Gallimberti 1972b).

(i) An ionic component I_+ due to motion of the active streamer head within the gap, with a phase velocity v_s.

(ii) An electronic component I_- due to motion of free electrons along the streamer filament with a drift velocity v_e.

Instantaneous values of these current components can be calculated if the instantaneous values of the associated quantities in equation (4) are known; however, the simplified streamer model gives only the final distributions of charge carriers as functions of the space coordinate x. The current calculation needs therefore a space–time relation, giving the time $t(x)$ associated with each position of the streamer head. This can be obtained by cumulation of the equivalent avalanche formative time t_f, which has been derived from previous, more sophisticated models (Badaloni and Gallimberti 1972, Gallimberti 1972b) as a function of N_s and E_g. The space–time relation $t(x)$ therefore results:

$$t(x) = \sum_i t_f(N_s(x_i), E_g(x_i)) \qquad x_i = 2iR \tag{5}$$

with the corresponding phase velocity of the streamer front:

$$v_s(x_i) = 2R/t_f(N_s(x_i), E_g(x_i)). \tag{6}$$

The ionic current can be expressed as follows:

$$I_+(t(x)) = \frac{eN_s(x)v_s(x)E_g(x)}{V_0}. \tag{7}$$

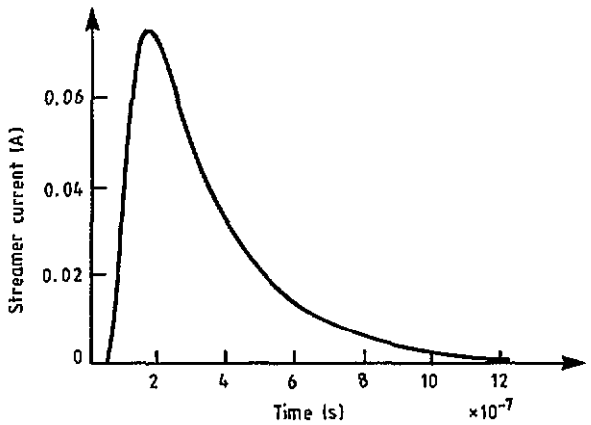

Figure 5. Computed current associated with the development of a single streamer filament (first corona). Same conditions as in figure 4.

Calculation of the electronic current component has to take into account the attachment of electrons drifting towards the electrode at velocity v_e. This leads to the following expression:

$$I_-(t(x)) = \int_{x_{lim}}^{x} \frac{ev_e}{2RV_0} E_g(y) N_s(y) \times \exp[-v_e(t(x) - t(y))]\,dy \qquad (8)$$

the integration limit x_{lim} being given by the equation

$$x_{lim} - v_e(t(x) - t(x_{lim})) = 0$$

which expresses the condition that electrons created at coordinates $x < x_{lim}$ have already been collected by the electrode and thus are not involved in the current at time $t(x)$. The computed current pulse associated with development of a single streamer filament is reported in figure 5; the total corona current is then obtained by multiplying by the branching factor f_b and the number of filaments N_f. Under the experimental conditions of figure 4 good agreement with experimental values is obtained when setting the branching factor to 5 and the number of filaments to 10.

6. Leader and second corona inception

6.1. Thermodynamic conditions for leader inception

At the first corona root ('stem'), the current flowing through the streamer filaments induces Joule heating of the gas. The streamer–leader transition is associated with the heating of the stem above a critical temperature, which corresponds to the thermal detachment of negative ions (1500–2000 K) and to a large increase of electronic density (Gallimberti 1979).

Those electrons that flow through the streamer channel without being attached will lose the specific energy EI by elastic and inelastic collisions with neutral species; I represents the current entering from the corona region into the stem. This energy is transferred to the molecules in different forms of internal

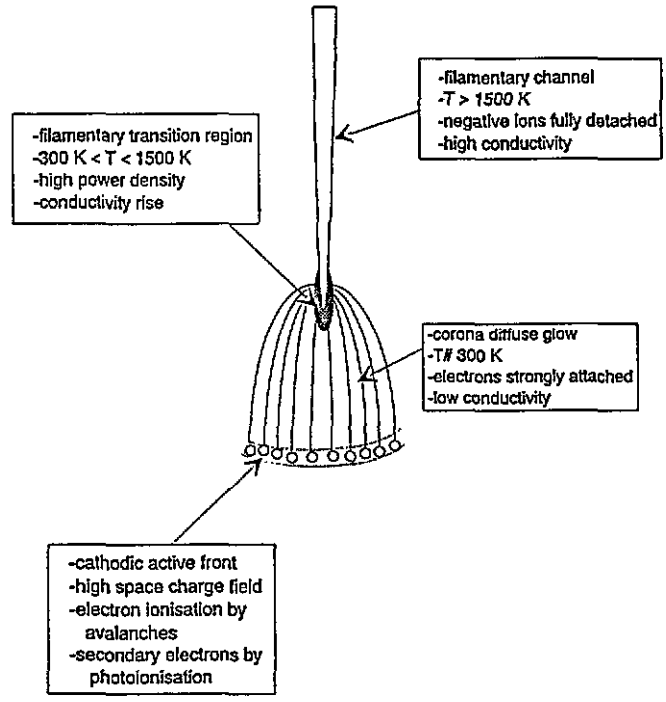

Figure 6. Geometry of the leader head.

energy: translation, rotation, vibration and electronic excitation. With E/n_h in the range 10^{-16}–10^{-15} V cm^2 (corresponding to the average field in a streamer filament), a large fraction $f_v = 0.95$ of the inelastic collision energy is transferred into vibrational excitation. The remaining part relaxes into translational form almost immediately with respect to the characteristic times involved in leader inception (Gallimberti 1979). The time constant τ_{vt} for relaxation of the vibrational energy into translational form is much longer (10^{-6}–10^{-4} s). It has been shown (Gallimberti 1979), using a cylindrical homogeneous model of the stem, that the time evolution of vibrational and translational temperatures can therefore be computed from the following equations:

$$\frac{d}{dt}\left(\frac{7}{2}kT_h n_h \pi a^2\right) = (f_e + f_r + f_t)EI + \frac{\pi a^2(\epsilon_v(T_v) - \epsilon_v(T_h))}{\tau_{vt}} \qquad (9)$$

$$\frac{d}{dt}(\pi a^2 \epsilon_v) = f_v EI - \frac{\epsilon_v(T_v) - \epsilon_v(T_h)}{\tau_{vt}} \pi a^2 \qquad (10)$$

where n_h is the density of neutrals, T_h and T_v are the translational and vibrational temperatures of neutrals, a is the stem radius, f_e, f_r, f_t, f_v are the fractions of the energy EI transferred to the molecules in the form of electronic, rotational, translational and vibrational excitation and ϵ_v is the vibrational energy per unit volume.

The numerical calculation is performed with the initial streamer channel conditions $R = 35$ μm and $T_v = T_h = 300$ K, using the current waveform obtained from simulation of the first corona. The

time for streamer–leader transition is reached when the translational temperature T_h becomes equal to the critical temperature $T_{crit} = 1500$ K.

Leader inception has been studied under various electrical configurations (Gallimberti 1979, Ulrich and Gallimberti 1988) and has given inception times in good agreement with the experimental measurements.

6.2. Electrical conditions for second corona inception

Actual inception and continuous propagation of the leader channel depends on the inception possibility of a second corona, which will constitute the active head of the streamer–leader system.

Owing to the existence of the stem and to the space charge left in the gap by the first corona, the electric field distribution along the gap axis is modified. The criterion for second corona inception is formally identical to the one derived in section 5.1 for first corona inception (equation (1)), taking into consideration the new field distribution. If this electrical condition is satisfied after fulfilment of the thermodynamical condition, then development of the second corona can be simulated as described in section 5.2.

7. Development of the streamer–leader system

7.1. Leader channel characteristics

Experimental results (Les Renardières Group 1972, 1974) have shown that the leader channel is a weakly ionized plasma channel, in which the energy input due to the flowing current induces significant thermo-hydrodynamic processes. A non-LTE model has been used (Gallimberti 1979) to analyse the balance of the different energy transfer processes, in order to calculate the channel expansion rate and the local electric field.

The thermal detachment of negative ions (which leads to a large conductivity increase at the channel tip), reduces the negative ion density almost to zero; therefore only three kinds of particles have to be considered in the leader plasma channel: electrons, positive ions and neutral particles.

This system of conservation equations for these three kinds of particles can be solved using a set of simplifying assumptions (Gallimberti 1979). It is then possible to obtain the reduced field along the leader channel, as a function of the current input:

$$\frac{E}{n_h} = \frac{I m_e a_e \nu_{eh}}{e^2 N_h \nu_i} \tag{11}$$

where ν_i is the ionization frequency, ν_{eh} is the electron–neutral species momentum transfer frequency and a_e is the total electron–ion recombination coefficient.

Equation (11) represents an implicit function that correlates the reduced field to the leader current, with the ratio ν_{eh}/ν_i and the value of a_e depending upon E/n_h only. Owing to steep variation of the ionization frequency with the reduced field, the conductivity and the degree of ionization are found to be almost proportional to the current; the reduced field on the contrary is almost constant over a wide range of current values (Gallimberti 1979). In typical laboratory conditions, the reduced field in the leader channel may be estimated as around 8×10^{-16} V cm^2.

Under the same assumptions, it has been shown (Les Renardières Group 1977) that the voltage drop along the leader channel can be calculated as

$$\Delta U_L = \frac{\gamma}{\gamma - 1} \frac{p\pi a_0^2}{\bar{q}_L} \left\{ \left[1 + 2 \left(\frac{E}{n_h} \right) \frac{n_0}{p\pi a_0^2} \bar{q}_L x_L \right]^{1/2} - 1 \right\} \tag{12}$$

where γ is the specific heat ratio, x_L the leader length and $\bar{q}_L$ the average charge per unit length

$$\bar{q}_L = \frac{1}{x_L} \int_0^t I \, dt \tag{13}$$

and n_0, a_0 are the initial neutral density and radius of the channel.

Equations (12) and (13) provide the value of the leader tip potential $U_{lt} = U_0 - \Delta U_L$, which is used in the field calculations during the streamer–leader system propagation.

7.2. Propagation of the streamer–leader system

The streamer–leader system, during the phase of its continuous propagation across the gap, may be represented (figure 6) as a coupled electric and thermodynamic instability wave giving rise to the dynamic transition from a diffuse glow to a filamentary arc (Gallimberti 1979). The streamer filaments converging into the leader tip may be represented as the positive column of a diffuse glow whereby the electrons, created at the active corona front, drift towards the abode. The streamer front acts as a moving cathode region, where the electrons extracted from the gas by photo-ionization multiply as avalanches, and create the space charge layer able to sustain the high field in the front region.

The current collected by the leader tip determines the energy input for the transition from diffuse glow to filamentary channel: the concentration of the current and field lines towards the leader tip produces a strong enhancement of the power input, which increases the local gas temperature above the critical temperature T_{crit} for negative ion detachment. Propagation of the leader tip in the gap sustains the electric field in the corona active front and hence supports the ionization phenomena necessary for streamer propagation.

The general development characteristics of the streamer–leader system are the result of strongly nonlinear coupling between the streamer activity and the leader tip advancement: if this coupling mechanism reaches an equilibrium situation, the streamer–leader system can propagate in a stable way across the gap.

The simulation of the streamer–leader development can be realized by a discretization of the time base (t_i,

$i = 0, 1, \ldots$) and a loop for step-by-step computation of all the coupled processes.

The different steps can be schematically described as follows.

(i) Calculation of the potential and field distribution on the gap axis at time t_i (section 4).

(ii) Computation of the advancement conditions of the leader corona: number of positive ions in the active front, propagation velocity and position (section 7.2.1).

(iii) Calculation of the current injected at the leader tip and of the space charge left in the gap (section 7.2.2).

(iv) Computation of the leader advancement velocity and position (section 7.2.3).

(v) Calculation of the leader channel characteristics, together with the total voltage drop and the tip potential (section 7.1.).

(vi) Determination of the new field and potential distribution at time t_{i+1}.

7.2.1. Leader corona advancement. According to the assumptions made in section 5, the corona front is described as a thin region of depth D_s including the active heads of the N_1 streamer filaments. If N_s represents the number of ions in each active head at time t, the streamer energy balance may be written in a simplified form (Gallimberti *et al* 1983):

$$\frac{dN_s}{dt} = \frac{N_s v_s}{U_g}\left(E_g - \frac{\beta - \mu E_g}{D_s}\right) \qquad (14)$$

with U_g the potential at the streamer front, E_g the external guiding field (including the geometric component, the leader component and the previous corona space charge) and v_s the streamer front advancement velocity.

The general streamer model proposed by Gallimberti (1972) shows that the streamer velocity depends essentially on the electric field in which the equivalent avalanche develops: it is the sum of the externally applied field and the local field due to the positive charge of the streamer heads. The velocity v_s depends linearly upon E_g and N_s. This leads to the following relation for the streamer acceleration:

$$\frac{dv_s}{dt} = \alpha_1(k_1 + k_2 v_s)(E_g - E_{gs}) + \alpha_2 \frac{dE_g}{dt}. \qquad (15)$$

Integration of this equation gives at any iteration the instantaneous value of the streamer advancement velocity v_s to be used in equation (14).

7.2.2. Leader current input. The current I_L calculated in this section corresponds to that flowing across the transition region during stable leader propagation at velocity v_L. It can be calculated using the same formalism described in section 5.2.2, with reference to the leader tip considered as a pseudo-electrode at potential U_{lt} (Gallimberti *et al* 1983).

Let us assume a reference frame moving into the gap with the same velocity v_L as the leader tip: in this frame, the leader corona region appears to have a quasi-stationary configuration. The active front contains the positive charge eN_1N_s of the N_1 streamer heads, which appears to move with a relative velocity $v_s - v_L$. It induces therefore a current component

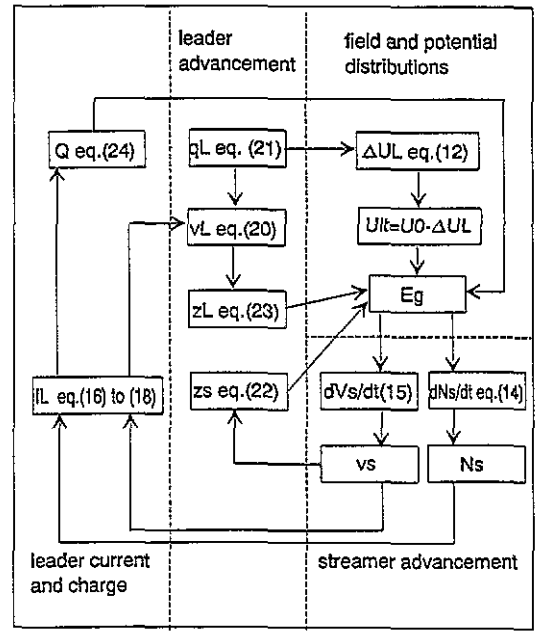

Figure 7. Flow-chart of the system of equations describing development of the streamer–leader system.

$$I_{Ls} = eN_1N_s(v_s - v_L)E_L(z_s)/U_{lt} \qquad (16)$$

where $E_L(z_s)$ is the value of the field produced by the leader pseudo-electrode at the streamer front.

The diffuse glow region contains the free electrons that are injected from the active front and move towards the leader tip at relative velocity $v_e + v_L$, until they remain attached. The electron current component has to be integrated over the whole glow region, taking into account that it decays exponentially because of attachment:

$$I_{L-} = \frac{eN_1N_s}{\eta D_s}(v_e + v_L)[1 - \exp(-\eta x)]\frac{\langle E_L\rangle}{U_{lt}} \qquad (17)$$

where x represents the streamer length and $\langle E_L\rangle$ the average field produced by the leader tip over the attachment mean free path $1/\eta$ behind the streamer front.

As the plasma in the glow region is essentially neutral, the free electrons are associated with an excess of positive ions (with respect to the negative ones), which has the same spatial distribution as the free electrons. In the moving reference frame, it appears to have a velocity v_L towards the leader tip and induces therefore a current component

$$I_{L+} = -\frac{eN_1N_s}{\eta D_s}v_L[1 - \exp(-\eta x)]\frac{\langle E_L\rangle}{U_{lt}} \qquad (18)$$

which reduces the corresponding electron component.

The total current input at the leader tip is the sum of the three components given by equations (16)–(18).

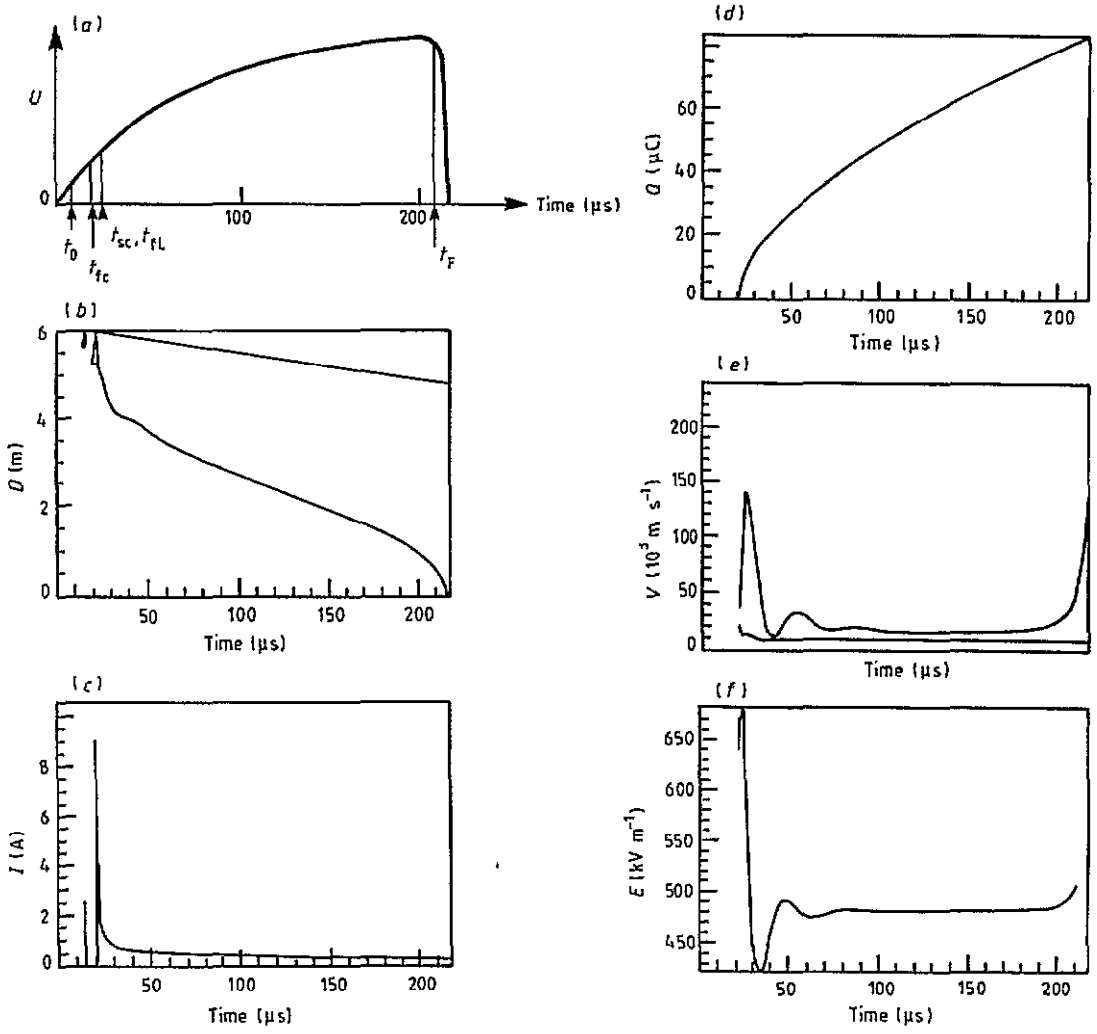

Figure 8. (*a*) Temporal evolution of the applied voltage. (*b*) Computed evolution of the space–time development of the positive spark (reference configuration D = 6 m, R_e = 0.6 mm and U_0 = 1550 kV). Characteristic times: t_0, time of minimum inception conditions, t_{fc}, time of actual first corona inception and development, t_{fL}, time of leader inception, t_{sc}, time of second corona inception and development and t_F, time for the beginning of the final jump. (*c*)–(*f*) Computed evolution of the discharge current, injected space charge, velocities of corona front and leader tip and electric field at the streamer tip.

7.2.3. Leader advancement. It has been shown (Gallimberti 1979) that a stationary leader tip propagation, in the form of a self-similar electric and thermal wave, is possible only if leader velocity in the conservation equations matches the temperature rise ΔT_h, from the ambient temperature T_0 up to the critical temperature T_{crit}.

Finally, the leader velocity can be calculated (Gallimberti 1979):

$$V_L = \left[f_e + f_r + f_t + f_v \frac{\langle \tau_L/\tau_{vt} \rangle}{1 + \langle \tau_L/\tau_{vt} \rangle} \right] \times \frac{2}{7 n_h (T_{crit} - T_0)} \int_{z_1}^{z_L} JE \, dz \qquad (19)$$

where E and J are the field and current density at the leader tip, z_L and z_1 are the coordinates of the leader and transition region limits, τ_L the leader transit time in the transition region $\tau_L = (z_L - z_1)/v_L$ and $\langle \tau_L/\tau_{vt} \rangle$ is the fraction of vibrational energy that is relaxed into thermal form in the transition region.

For an easier calculation of the integral term $\int_{z_1}^{z_L} JE \, dz$, the leader head is represented as a slender paraboloid surface of curvature radius ρ_c, whereas the corona region is represented by a confocal paraboloid sector η_0 (Gallimberti 1979).

Under these assumptions it can be shown that the propagation velocity is found to be proportional to the leader current:

$$v_L = I_L/q_L \qquad (20)$$

through a constant

$$q_L = \frac{14\pi \eta_0^2 \rho_c \log[(\rho_c/2D)]^{1/2} k n_h (T_{crit} - T_0)}{U_{lt} \log\left(\frac{2(z_L - z_1)}{\rho_c}\right) \left(f_t + f_r + f_e + f_v \frac{\langle \tau_L/\tau_{vt} \rangle}{1 + \langle \tau_L/\tau_{vt} \rangle} \right)} \qquad (21)$$

which represents the charge per unit length necessary to realize the thermal transition from the diffuse glow to the filamentary leader channel.

Table 1.

Time	Action	Formulae	Results
$t = 0$	Start voltage wave		
$0 < t < t_0$	Testing first corona inception conditions	(1)	Ionization integral < 18
$t = t_0$	Minimum inception conditions reached at time t_0	(1)	$t = 5.0\ \mu s$ $U = 182$ kV $E_g = 60.2$ kV cm^{-1} Ionization integral = 18
$t_0 < t < t_{fc}$	Statistical delay		$\Delta t = 5.0\ \mu s$
t_{fc}	Development of first corona	(2)–(8)	$t = 10.0\ \mu s$ $X_s = 38$ cm $Q = 0.69\ \mu C$ $I_{peak} = 2.8$ A
$t_{fc} < t < t_{fL}$	Testing leader thermodynamic inception condition	(9) and (10)	
t_{fL}	Thermodynamic condition reached at time t_{fL}		$t = 15.1\ \mu s$ $T_h = 1500$ K $T_v = 23320$ K
$t_{fL} < t < t_{sc}$	Testing second corona inception conditions	(1)	$t = 15.1\ \mu s$ Ionization integral = 161
t_{sc}	Development of second corona	(2)–(8)	$t = 15.1\ \mu s$ $X'_s = 88$ cm $Q' = 6.2\ \mu C$
$t_{sc} < t < t_F$	Development of streamer–leader system	(11)–(24)	Z_s, Z_L, E_{gs} v_s, v_L, U_{lt} Q, I_L, I_c see figure 15
$t_{sc} < t < t_F$	Test of leader arrest conditions	$v_s > v_{smin}$ $N_s > N_{stab}$ $Z_s(t) > 0$	
t_F	Breakdown or discharge arrest		$t = 222\ \mu s$ Breakdown

7.2.4. Leader and streamer positions. The position of the corona front z_s may be obtained from integration of the velocity equation (15):

$$z_s = z_{s0} - \int_0^t v_s \, dt \tag{22}$$

with z_{s0} the second corona limit coordinate.

It should be noted that $x_L = \int_0^t v_L \, dt$, with v_L derived from equation (20), provides the value of the actual length of the leader channel along its tortuous path. In order to calculate the leader tip position z_L it is necessary to introduce a tortuosity coefficient ψ, which represents the randomness of the leader path. Average values of ψ have been experimentally determined (Les Renardières Group 1977) and theoretically calculated (Gallimberti 1979). The leader tip coordinate is then

$$z_L = D - x_L/\psi. \tag{23}$$

7.2.5. Space charge. The net positive charge left in the gap by the leader propagation is

$$Q = \int_0^t I_L \, dt. \tag{24}$$

It represents the increase of space charge during the leader streamer system propagation, starting from the initial value Q_s given by the corona phase.

The total charge $Q + Q_s$ has to be introduced in calculation of the field and potential distributions along the gap axis.

7.2.6. Conditions for unstable propagation and discharge arrest. Equations (11)–(24) represent a consistent set of coupled analytical equations, which can be solved numerically with a finite-difference procedure. In figure 7, a flow-chart of the procedure is reported, indicating the correlation between different variables of the model. The initial conditions are derived from the general programme, which simulates sequentially the conditions for inception and development of the first corona, inception of the leader, and inception and development of the second corona (see figure 2).

In order to complete the computation, various conditions of arrest or instability of the discharge have to be taken into account.

(i) The first one corresponds to arrival of the corona front at the grounded plane (breakdown condition); the arrest criterion is then given by the condition $Z_s(t) = 0$.

(ii) The second one is associated with the energy balance for leader corona advancement: if the number

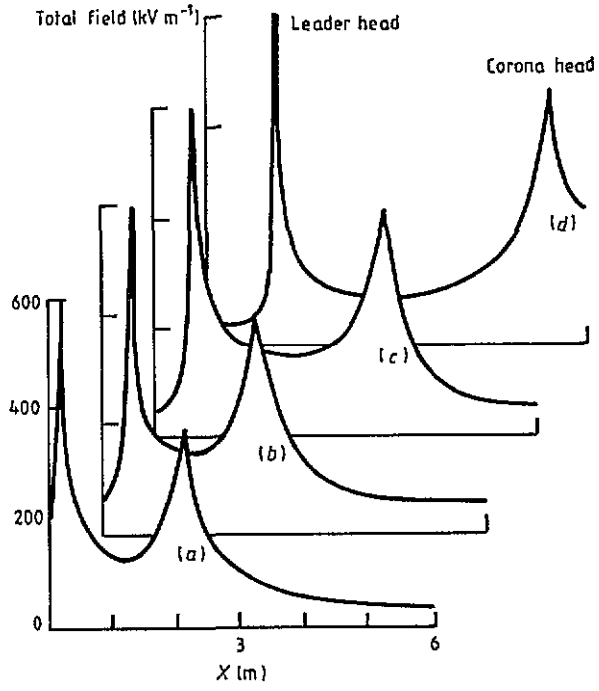

Figure 9. Temporal evolution of the field distribution for different positions of the discharge in the gap, with indication of the leader and corona head positions. Same configuration as in figure 8. $t = 50$, 100, 150 and 200 μs for curves (*a*)–(*d*).

of ions N_s contained in the head of the streamers becomes lower than the stability charge value N_{stab}, stable reproduction of the ionization processes is no longer possible. The comparison of N_s and N_{stab} is then performed at each time step.

(iii) The third one is associated with dynamic coupling between the corona and leader tip advancements: under specific circumstances the streamer velocity may go to zero, arresting the current feed to the leader tip. The fulfilment of the condition $v_s(t) > 0$ is checked at every time step.

8. Results

8.1. General description of the computation

A detailed description of the results is given here in the case of a conic (curvature radius $R_e = 0.6$ mm) rod–plane gap of length $D = 6$ m, subjected to a positive voltage impulse of crest level $U_0 = 1550$ kV (equal to the U_{50} value resulting in 50% cases of breakdown). The time to crest is 240 μs, and the time to half value of the voltage tail is 9000 μs. The corresponding voltage waveform is given in figure 8(*a*), with indication of the different characteristic times of the discharge development. With reference to these characteristic times, the different stages of the computation are described in table 1. At each step the programme computes a new field distribution, due to the injection of new space charge (formation of coronas or development of the streamer–leader system), and to evolution of the leader tip potential. Then, it simulates the different

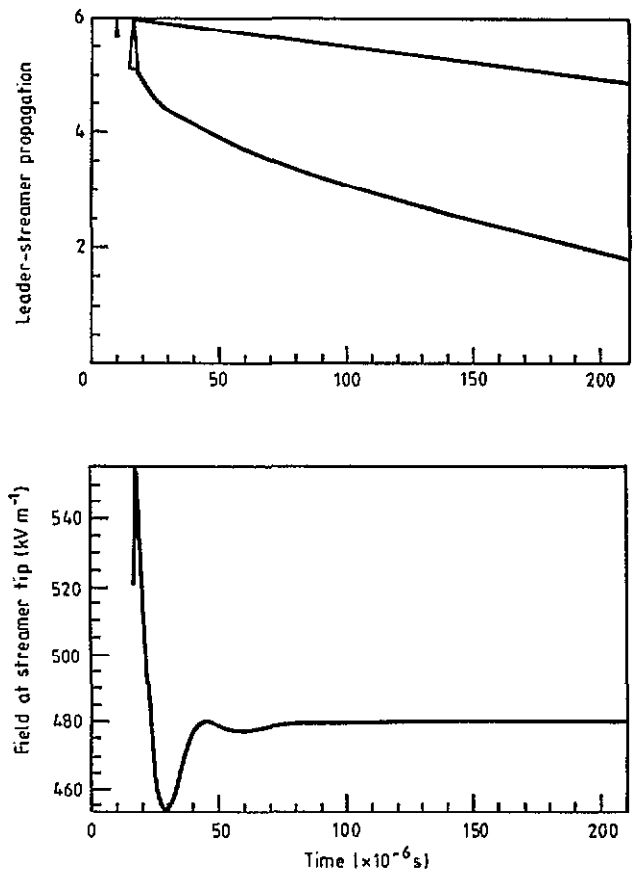

Figure 10. Computed space–time development of the discharge at $0.95U_{50}$ ($D = 6$ m, $R_e = 0.6$ mm) and associated electric field at the streamer tip.

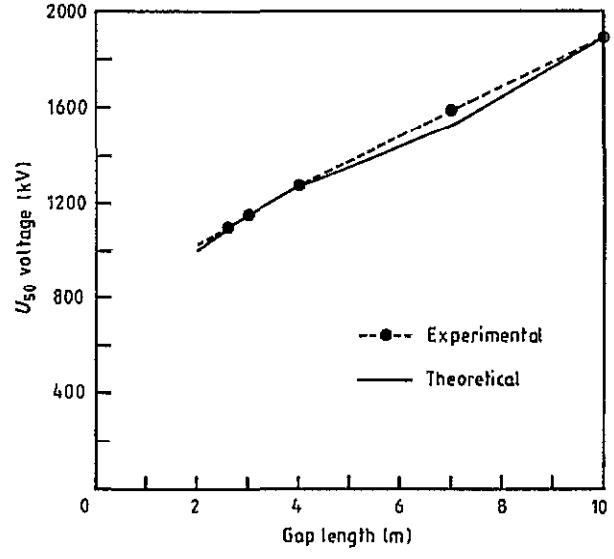

Figure 11. Experimental and computed values of voltage U_{50}, as a function of gap length D (electrode curvature radius $R_e = 0.6$ m and voltage impulse waveform 320/10 000 μs).

development phases by using the specific equations listed in the present paper. The numerical output of each step of the model (table 1) is used as an input in the subsequent computation subroutine.

The computed evolution of the discharge development is given in figure 8(*b*), on a space–time representation similar to a streak cameragram: the various

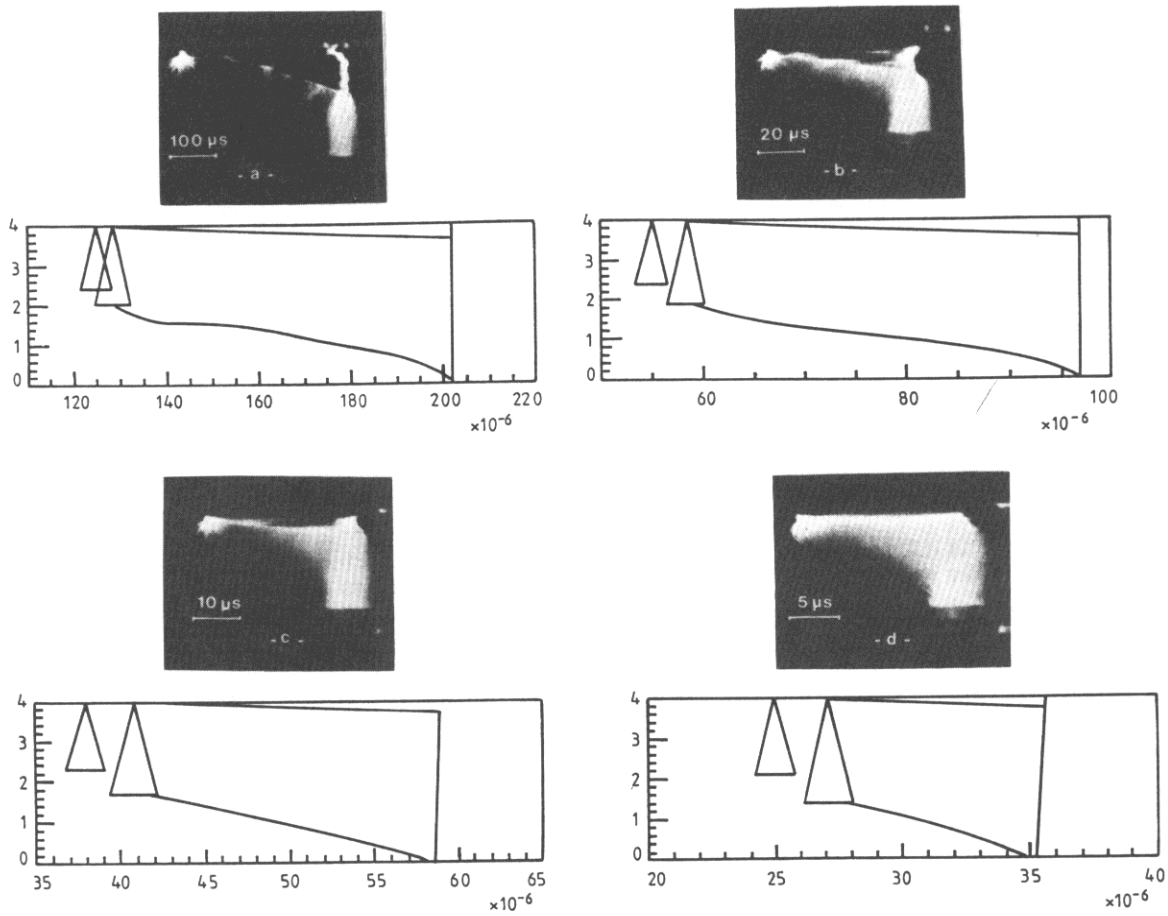

Figure 12. (*a*)–(*d*) Streak photographs and computed space–time development of the discharge for voltage crest values ranging from U_{50} to $3.3U_{50}$ (gap length $D = 4$ m, electrode curvature radius $R_e = 0.6$ m and voltage impulse waveform 320/10 000 μs).

stages of the discharge development appear in figure 8. Note that the formation and development of first and second corona (times t_{fc} and t_{sc}) are represented there as static triangles owing to the high velocity of coronas development with respect to the time scale of the whole discharge development.

Figures 8(*c*)–(*f*) give the computed evolution of the associated current, velocities of corona and leader, injected space charge and electric field at the streamer tip. The computed current evolution is consistent with experimental measurements and shows sharp current pulses associated with corona formation, followed by a low continuous current (about 1 A), associated with propagation of the leader discharge. The streamer front advances with oscillating velocity, until the total guiding field reaches a stable condition around the energetic stability value. Figure 9 gives the temporal evolution of the distribution of axial electric field at different propagation times.

8.2. Calculation of the 50% breakdown voltage U_{50}

The model enables calculation of the U_{50} voltage for a given electrode configuration. It has been experimentally shown that most of the statistical dispersion of the breakdown process is related to the random tortuous path of the leader channel, which is represented in the model by the tortuosity coefficient ψ (section 7.2.5). With an average empirical value of ψ, by successive attempts, it is possible to determine the limit crest voltage value U_0 that leads to breakdown under average statistical leader conditions: it corresponds therefore to U_{50}. At lower voltage values (see figure 10) the arrest condition $N_s(t) < N_{stab}$ is obtained during discharge propagation, because the input of electrostatic energy at the active head of the discharge is not sufficient to sustain streamer–leader propagation up to the opposite plane.

The computed values of U_{50} have been compared with experimental results obtained on rod–plane gaps in the range 2–10 m (hemispherical electrode tip of 0.6 m diameter) subjected to positive switching impulses of 320–10 000 μs (Baldo *et al* 1975): figure 11 presents this comparison as a function of the gap length D.

8.3. The effect of overvoltage on the propagation characteristics

For a given electrode configuration, the discharge development in space and time is strongly influenced by the overvoltage applied to the gap. Figures 12(*a*)–(*d*) present the streak photographs of the discharge for 4 m

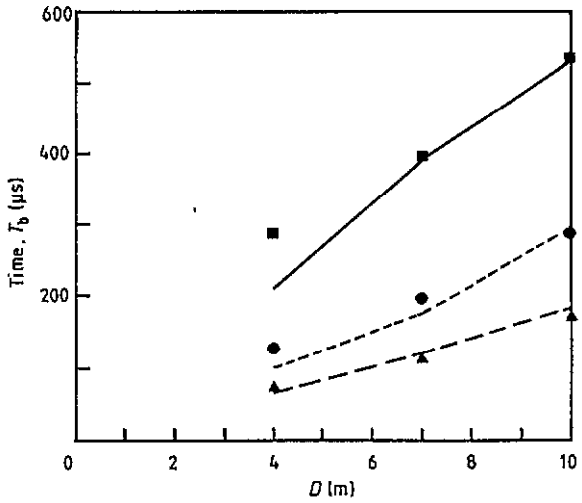

Figure 13. Experimental (■, U_{50}; ●, $1.6U_{50}$; and ▲, $2.2U_{50}$) and computed (lines) time to breakdown T_B, as functions of the gap length and voltage crest (electrode curvature radius $R_e = 0.6$ m and voltage impulse waveform 320/10 000 μs).

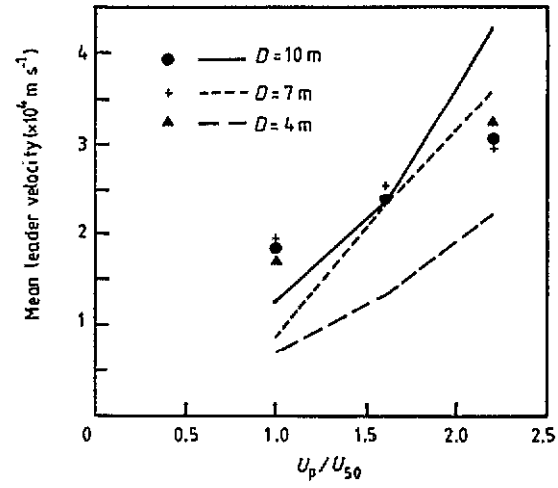

Figure 14. Experimental and computed (lines) mean axial velocity v_L, as functions of the gap length and voltage crest (same conditions as in figure 13).

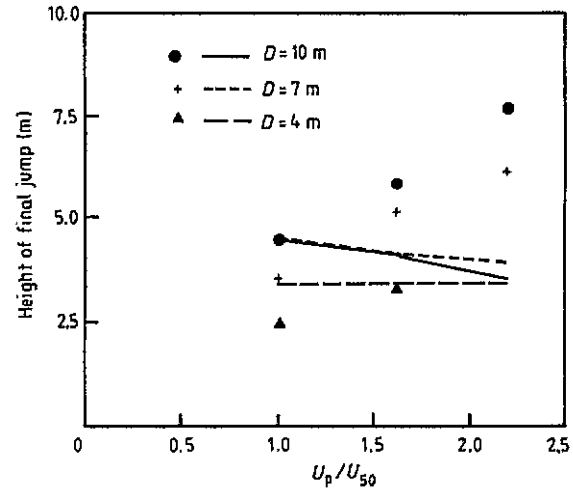

Figure 15. Experimental and computed (lines) heights of the final jump h_f, as functions of the gap length and voltage crest (same conditions as in figure 13).

gap length, in the experimental conditions described in section 8.2, for voltage crest values ranging from U_{50} to $3.3U_{50}$. The corresponding numerical simulations were performed using the following input parameters.

(i) The statistical time delay before the first corona inception is deduced from experimental values reported by Baldo *et al* (1975).

(ii) The number N_f of filaments in the corona region is chosen in the range 30–50, depending on the voltage crest value, consistent with reported experimental observations.

The computed space–time evolution of the discharge is given in figures 12(*a*)–(*d*). The computed time to breakdown T_B, mean leader axial velocity v_L, and height of the final jump h_f (leader axial length at time T_B) are reported in figures 13, 14 and 15 respectively as functions of gap length D and crest voltage U_0, together with the corresponding experimental results. The calculated times to breakdown are in good agreement with experimental values. The computed leader velocities are roughly consistent with the measured ones although the dependence on overvoltage is stronger for experimental values than for the predicted ones. The calculated heights of final jumps are almost constant with overvoltage, while the measured values increase with the U_0/U_{50} ratio; however, this discrepancy does not affect strongly the overall agreement between the model and experimental results. It appears that the model gives a good description of the physical conditions of discharge development over a wide range of experimental conditions, leading to predictive calculations of inception voltages, 50% breakdown voltages, and times to breakdown.

8.4. Dynamics of the streamer–leader system: effect of voltage perturbations

The influence of voltage front perturbation on discharge development has been extensively studied by the Les Renardières Group (1986). A double impulse test programme was performed using a rapid perturbation wave (2/30 μs front and tail), superimposed at different times on a switching impulse (240/9000 μs). The electrode configuration is the same as that described in section 8.1. Streak cameragrams and electrical measurements were used to analyse the effect of voltage perturbation on the leader propagation phase. Experimentally, it has been observed that the dynamics of the streamer–leader system is very different depending on the time at which the perturbation is applied.

(i) When the perturbation is applied in the early stages (t_p = 30 μs) of discharge propagation, the global effect is very small and the discharge returns rapidly to its unperturbed behaviour; breakdown time and probability remain unchanged (the corresponding streak photograph is given in figure 16(*a*), for a basic pulse of crest voltage $U_0 = 1550$ kV and a perturbation of crest voltage $U_{p0} = 800$ kV).

(ii) When the pulse is applied at intermediate times (t_p = 90 μs), the reaction of the system is much

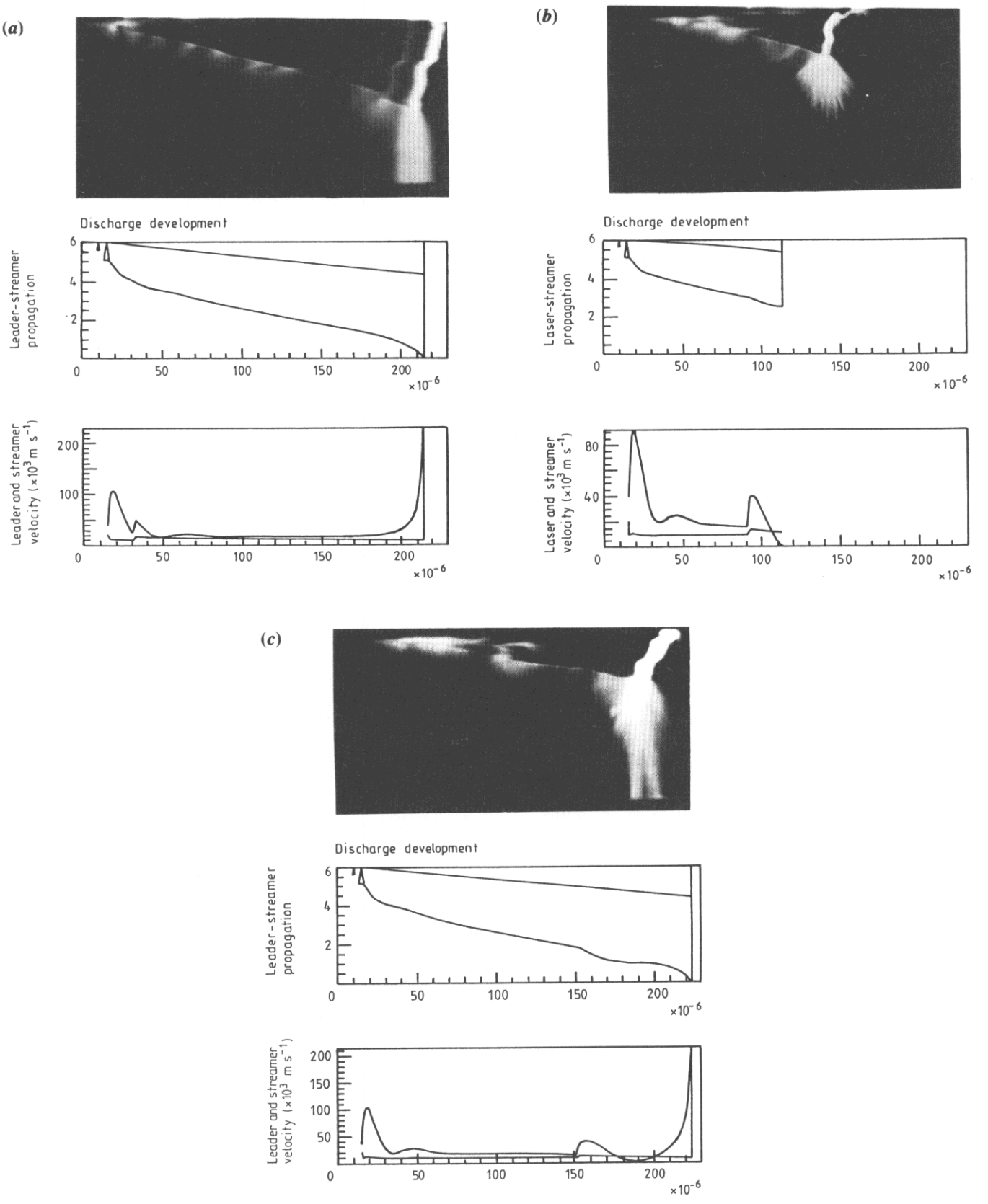

Figure 16. (*a*) Streak photograph, computed space–time development and velocity of the discharge with application of a voltage perturbation at time $t_p = 30$ μs. Configuration: $D = 6$ m, $R_e = 0.6$ mm, basic positive voltage $U_0 = 1550$ kV, basic voltage waveform 240/9000 μs, perturbation voltage crest $U_{p0} = 800$ kV and perturbation waveform 2–30 μs. The number of filaments N_f is set to 10 and the branching factor f_b is set to 5. (*b*) Streak photograph, computed space–time development and velocity of the discharge with application of a voltage perturbation at time $t_p = 90$ μs. Same configuration as in (*a*). (*c*) Streak photograph, computed space–time development and velocity of the discharge with application of a voltage perturbation at time $t_p = 150$ μs. Same configuration as in (*a*).

stronger. The leader corona size increases abruptly, the leader advances in a rapid jump but this is immediately followed by complete extinction of the discharge. No breakdown is then observed (figure 16(*b*), same voltage conditions as figure 16(*a*)).

(iii) When the perturbation is applied at later stages ($t_p = 150$ μs), the discharge is significantly accelerated and develops rapidly to the final jump (figure 16(*c*), same voltage conditions as figure 16(*a*)).

The model has been tested in the three above cases, and the corresponding computed results are reported in figures 16(*a*)–(*c*). The basic mechanisms that determine the discharge behaviour under voltage perturbation can be summarized as follows.

(i) For $t_p = 30$ μs, the perturbation induces an increase of streamer velocity and an elongation of the streamer front resulting in a decrease of the field E_g at the corona front; however, due to the high rate of rise of the applied voltage at this time, the field E_g is rapidly restored and the streamer–leader system recovers stable propagation conditions.

(ii) For $t_p = 90$ μs, the leader conductivity and the space charge are higher and streamer elongation leads to a more significant reduction of the field E_g. This leads to a rapid decrease of the streamer velocity, followed by a decrease of the leader velocity itself; at that time, the rate of rise of the voltage wave is much smaller and the field at the active front cannot recover fast enough. The streamers then continue to slow down until complete arrest of the discharge.

(iii) For $t_p = 150$ μs, propagation of the streamer–leader system is mainly governed by the space-charge field, which gives the major contribution to E_g. At this late stage the corona front is close to the grounded plane and the field E_g increases rapidly because of the increasing contribution of the image charge in the plane. Elongation of the streamers due to voltage perturbation directly results in an increase of velocity sufficient for the corona front to reach the plane and start the final jump.

The computed results are in good agreements with reported experimental observations and the physical basis of the model allows a satisfactory interpretation of the discharge dynamics under perturbed voltage conditions.

9. Conclusion

The proposed model is based on simplified simulation of the successive phases of discharge development; use of analytical computation methods enables implementation on personal computers. The proposed model has been successfully tested over a wide range of experimental conditions, for different electrode configurations, gap lengths, overvoltages and voltage waveforms. Comparisons with experimental data indicate that this self-consistent model can also take into account dynamic aspects of the discharge behaviour, such as its response to a transient voltage perturbation.

The growing practical interest in self-consistent modelling of lightning discharges gives rise to a new set of applications for the model proposed here. As the model uses mainly the initial electric field distribution as an input, its adaptation to simulation of lightning processes could be performed using the same computation methods. However, further work is needed for analysis of the specific mechanisms due to the higher current and fields involved in the lightning case.

References

Badaloni S and Gallimberti I 1972 The inception mechanism of the first corona in nonuniform gaps *Padova University Report UPee* 72/03

—— 1973 Monte Carlo simulation of streamer branching *XI Int. Conf. On Phenomena in Ionized Gases, Praha*

Badaloni S, Gallimberti I and Marode E 1992 A simplified model of streamer formation in weakly electronegative gases, unpublished

Baldo G, Gallimberti I, Garcia H N, Hutzler B, Jouaire J, Simon M F 1975 Breakdown phenomena of long gaps under switching impulse conditions. Influence of distance and voltage level. *IEEE Trans. Power Appar. Syst.* **94**

Dawson G and Winn W P 1965 A model for streamer propagation *Z. Phys.* **183** 159–71

Gallimberti I 1972a *J. Phys. D: Appl. Phys.* **5** 2179–89

—— 1972b Mathematical model for streamer formation in non uniform gaps *Padova University Report UPee* 72/04

—— 1979 The mechanism of long spark formation *J. Physique Coll.* **40** C7 Suppl. 7 193–250

Gallimberti I, Goldin M and Poli E 1982 *Padova University Report UPee* 82/07

—— 1983 Electric field calculation in long gap discharges *4th Int. Symp. on High Voltage Engineering, Athens 5–9 September*

Hartmann G 1977 Spectroscopies de la décharge couronne *PhD Thesis* Paris

Les Renardières Group 1972 *Electra* **23** 53–157

—— 1974 *Electra* **35** 49–56

—— 1977 *Electra* **53** 3–153

—— 1981 *Electra* **74** 67–216

—— 1986 *IEE Proc.* A **133**

Loeb L and Meek J M 1941 *The Mechanism for Electric Spark* (Stanford, California: Stanford University Press)

Marode E 1972 La formation de l'arc entre une pointe positive et un plan *PhD Thesis* Paris

—— 1975 The mechanism of the spark breakdown in air at atmospheric pressure between a positive point and a plane. I. Experimental: nature of the streamer track. II. theoretical: computer simulation of the streamer track *J. Appl. Phys.* **46** 2005–20

Marode E, Bastien F and Bakker M 1979 A model of the streamer induced spark formation based on neutral dynamics *J. Appl. Phys.* **50** 140

Marode E, Hilhorst D, Gallimberti B and Gallimberti I 1978 The radial distribution of space charge in a filamentary discharge *Gaseous Electronic Conf. Buffalo, New York*

Meek J M and Craggs J D 1978 *Electrical Breakdown of Gases* (New York: Wiley)

Phelps C T 1971 Field enhanced propagations of corona streamers *J. Geophys. Res.* **76** 5799-806

Raether H 1939 Die Entwicklung der Elektronenlawine in den Funkenkanal *Z. Phys.* **112** 464–89

Ross J N 1977 The diameter of the leader channel using Schlieren photography *Electra* **53** 71–3

Ullrich L and Gallimberti I 1988 A numerical inception model in air: experimental results and model predictions *IXth Int. Conf. on Gas discharges and their Applications, Venezia, 19–23 September*